BNL-213632-2020-JAAM

Ordered three-dimensional nanomaterials using DNA-prescribed and valence-controlled material voxels

Y. Tian, O. Gang

To be published in "Nature Materials"

January 2020

Center for Functional Nanomaterials

Brookhaven National Laboratory

U.S. Department of Energy

USDOE Office of Science (SC), Basic Energy Sciences (BES) (SC-22)

Notice: This manuscript has been authored by employees of Brookhaven Science Associates, LLC under Contract No. DE-SC0012704 with the U.S. Department of Energy. The publisher by accepting the manuscript for publication acknowledges that the United States Government retains a non-exclusive, paid-up, irrevocable, world-wide license to publish or reproduce the published form of this manuscript, or allow others to do so, for United States Government purposes.

DISCLAIMER

This report was prepared as an account of work sponsored by an agency of the United States Government. Neither the United States Government nor any agency thereof, nor any of their employees, nor any of their contractors, subcontractors, or their employees, makes any warranty, express or implied, or assumes any legal liability or responsibility for the accuracy, completeness, or any third party's use or the results of such use of any information, apparatus, product, or process disclosed, or represents that its use would not infringe privately owned rights. Reference herein to any specific commercial product, process, or service by trade name, trademark, manufacturer, or otherwise, does not necessarily constitute or imply its endorsement, recommendation, or favoring by the United States Government or any agency thereof or its contractors or subcontractors. The views and opinions of authors expressed herein do not necessarily state or reflect those of the United States Government or any agency thereof.

Ordered three-dimensional nanomaterials using DNA-prescribed and valence-controlled material voxels

Ye Tian,[1, 6] Julien R. Lhermitte,[1] Lin Bai,[2] Thi Vo,[3] Huolin L. Xin,[1] Huilin Li,[2] Ruipeng Li,[4] Masafumi Fukuto,[4] Kevin G. Yager,[1] Jason S. Kahn[3], Yan Xiong[3], Brian Minevich[3], Sanat K. Kumar,[3] and Oleg Gang[1,3,5,]*

[1]Center for Functional Nanomaterials, Brookhaven National Laboratory, Upton, NY, 11973, United States

[2]Van Andel Institute, Grand Rapids, MI, 49503, United States

[3]Department of Chemical Engineering, Columbia University, New York, NY, 10027, United States

[4]National Synchrotron Light Source II, Brookhaven National Laboratory, Upton, NY, 11973, United States

[5]Department of Applied Physics and Applied Mathematics, Columbia University, New York, NY 10027, United States

[6]College of Engineering and Applied Sciences, Nanjing University, Nanjing, 210093, China

* Email address: og2226@columbia.edu

The ability to organize nanoscale objects of various kinds into well-defined three-dimensional (3D) arrays can translate advances in nanoscale-synthesis into targeted material fabrication. Despite successes in nanoparticle assembly, most extant methods are system-specific. The problem of organizing biomolecules in 3D ordered arrays is even more challenging due to their complex shapes and surface chemistry. Here, we demonstrate experimentally and computationally a platform strategy for creating 3D ordered arrays of diverse types from nanoobjects of different kinds. In our assembly approach, 3D lattices are built from DNA prescribed and valence-controlled *material voxels (*termed *DNA material voxels)*. These *DNA material voxels* integrate nano-objects that carry material property with 3D DNA frames, allowing an object's valence and coordination to be determined by the frame's vertices that are capable binding with each other through hybridization. Consequently, DNA material voxel defines the lattice symmetry through the spatially-prescribed valence. This strategy offers a complete decoupling of a three-dimensional assembly process from the nature of components. Thus, the same assembly process can be applied and the same superlattice can be formed for inorganic and bio-organic nanocomponents of different intrinsic properties and shapes, as we show for metallic and semiconductor nanoparticles as well as for proteins. We further demonstrate a utility of this assembly method for creating light-emitting 3D arrays with diffraction-limited spectral purity and 3D enzymatic arrays with increased activity.

Self-assembly relies on a combination of inter-object interactions and an object's specific shape to achieve a system organization. The significant progress in designing shells and shapes of nanoscale objects provides a playground for exploring and understanding these relationships and to map out the resulting phases.[1-6] Despite significant progress in this field, it is challenging to create *desired* organizations from *specific* nano-objects due to an intrinsic problem – a coupling between the properties of the objects and the resulting organization. Thus, from a material design point of view, nearly each system requires its own solution. The problem of forming ordered structures is even greater for biomolecules due their complex shapes and distributions of surface groups. While for the two-dimensional assemblies, surface patterning can be often used for scaffolding nano-objects, there is no viable option for building three-dimensional (3D) ordered arrays with the desired organizations.

In the last decades, DNA emerged, as was proposed by Seeman in 1982[7], as a polymer capable of defined structural organization at small scales. Moreover, in this context, DNA is a precisely programmable material[8-11] appropriate for directing 3D particle organization[12-16]. Typically, particles are bound with single-stranded DNA chains, and assembled using base-pairing of complementary sequences. This robust approach, however, cannot decouple particle properties, e.g., its shell, size, shape, from the assembly structure. The problem of organizing biomolecules even greater. Thus, an outstanding challenge is to establish platform approaches for assembly of nanoscale objects of different nature in 3D.

Here we tackle this challenge by using 3D DNA frameworks formed from polyhedral DNA frames for organizing nano-objects that are contained inside frames. The versatility of this approach should extend to catalytic, biological and inorganic matrices[17], metamaterials[18], and information storage devices[19]. One of the key difficulties in realization of this strategy is to reveal relationship between the design of frame and inter-frame connectivity, and formation of 3D ordered framework. To date, a successful approach has used DNA strand sets forming tensegrity triangles to precisely assemble 3D DNA molecular crystals[20]. These crystals can incorporate

organic semiconductors[21] or DNA devices[22]. However, the lattice type is limited to that motif and the small guest species (<7 nm). Recently, DNA origami[9,23] in a format of tensegrity triangle was used to reproduce this type of lattice through stacking interactions and to host nanoparticles[24]. Here, we use DNA origami frames of different shapes, as we discuss below, to both host desired nano-objects and access different lattice symmetries through vertex-to-vertex hybridization of frames. Unlike stacking, hybridization permits a great control over interactions encoding, energetics and flexibility of interframe linkages. Although co-assembly of lattices of spherical nanoparticles and DNA frames of different shapes has been demonstrated[15,16], lattice formation in such approach depends on the intricate balance of maximizing a number of particle-to-frame hybridization and minimizing interframe interactions; thus, formation of lattice is highly depends of the particle properties. In contrast, in this work, we demonstrate that 3D ordered lattice can be fully assembled purely from DNA frames with shapes of Platonic solids, such as a tetrahedron, octahedron, and cube.

In our approach, polyhedral frames are capable of inter-frame hybridization only via vertex-to-vertex hybridization (Figure 1). Thus, the DNA frame possess a spatially determined valence (v) defined by its shape. Inter-frame hybridization results in assembly with the ability to form an ordered lattice, whose type is determined by the frame valence. The frame might be empty or enclose nano-objects (e.g., nanoparticles, proteins), correspondingly resulting in the formation of empty DNA framework or arrays of precisely positioned nano-objects. Such strategy allows us to use the same assembly process for creating arrays of very different types of nano-objects (inorganic nanoparticles and proteins), since this assembly approach intrinsically decouples a formation of a lattice from the nano-objects with a specific materials identity (Fig. 1, left). The DNA frame with nano-object inside (Fig.1, middle) represents a building block for the formation of 3D lattice (Fig.1, right). This block has a specific *valence* determined by the vertices of DNA-frame and carries a specific nanomaterial object inside, thus, we term it *DNA material voxel*. Instead of typical optical signature associated with pixel terminology, *DNA material voxel is an elementary volumetric*

block carrying material property and its binding characteristics fully determined by frame shape that lead to a 3D nanomaterial lattice.

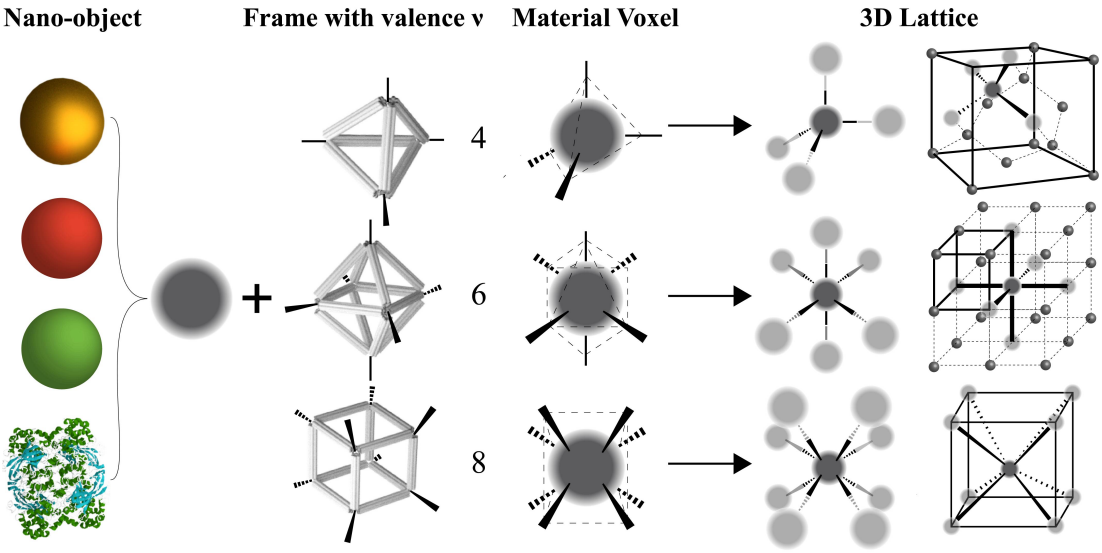

Figure 1. Schematic of the DNA material voxels platform for assembly of 3D lattices from inorganic (nanoparticles) and bioorganic (proteins) nano-objects with DNA frames. Tetrahedra, octahedra and cubic have correspondingly valence v=4, 6 and 8, and their respective edge-lengths in this study are about 36, 29, and 29 nm.

We first discuss 3D DNA origami lattices formed from octahedral frames (valence v=6, edge length is about 29 nm) containing twelve 6-helix-bundle edges (6HB, see Supplementary Material), designed with caDNAno[23]. Each octahedron vertex (OB) incorporates single stranded (ss) DNA motifs with $l+m$ free bases (blue, Figure 2a). This construction allows for hybridization of m nucleotides with complementary strand fragments ($n+m$ free bases, red in Figure 2a) on another octahedron (OR) (Table S1). The vertex-driven 6-fold octahedral valency should yield ordered assemblies through vertex-to-vertex hybridization of frames, which we probe by Small Angle X-ray Scattering (SAXS) and understand by comparing to a validated model[25] accounting for the nano-object's form factor, DNA bundle arrangement, and the lattice type (Supplementary Material). For the octahedral frame assemblies (l=22, m=22, n=8; no encapsulated nano-objects), the 2D SAXS pattern and the corresponding structure factor, S(q) (q - scattering vector), reveal a remarkably well-ordered simple cubic (SC) lattice with 15 orders of resolution-limited Bragg peaks (Figure 2b, black for data, red

for model). Negative-stained TEM (Figures 1c and S2) reveals domain sizes of 3–5 μm. While formation of stand-alone DNA framework offers proof-of-concept for this design approach, more relevant is to template nano-object organization into 3D arrays. Thus, we first sequester 10 nm gold nanoparticles (AuNP) inside DNA octahedra before these material voxels self-assemble (Figure 3a, R1). AuNPs are positioned in the middle of each octahedron by hybridization with its internal strands (Figure 3b). We then mix OB and OR frames (with encaged AuNPs) and anneal to form a templated 3D AuNP array, confirmed by cryo-scanning transmission electron microscopy (STEM) (Figures 3c and S18) and ~25 SAXS diffraction peaks (Figure 3e, black curve). The ratios of SAXS peak positions $q/q_1 = 1: \sqrt{2} : \sqrt{3}: 2\ldots$ correspond to a AuNP SC lattice, consistent with the templating lattice. S(q) modelling (Fig. 3e, red; Supplementary Material) confirm the lattice type, long-range order, and high-fidelity SC packing of origami templates (Figure 3a). Further, the lattice parameters, corresponding to the empty ordered DNA framework (Figure 2a), confirm templating.

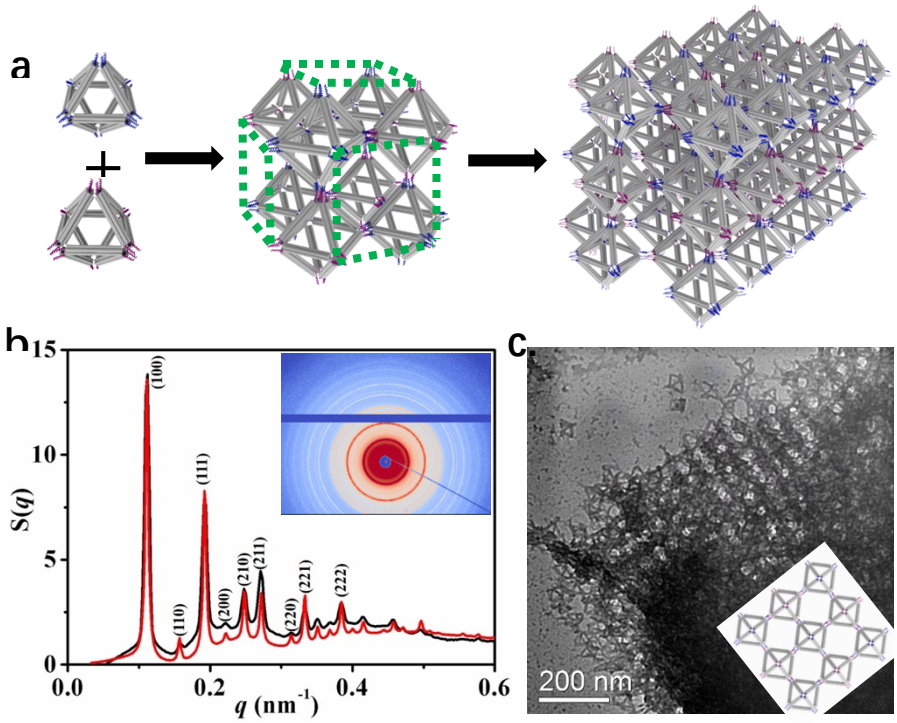

Figure 2. Assembly of octahedra frames into DNA lattice. (a). ssDNA encoded octahedral frames OB and OR (left) with complementary strands (blue and red) were mixed to form a DNA lattice (right). The unit cell (center) with green dotted lines shows three faces of the unit cell. (b). Measured 2D SAXS pattern (inset) and corresponding structure factor, S(q), for 3D

DNA lattice (black curve) and a fit modelled using a SC lattice of DNA octahedra (red curve). (c). Representative negative stained TEM image (scale bar: 200 nm) for DNA lattice formed by DNA octahedra; overlay shows the corresponding lattice orientation.

AuNP arrays can also be formed *post facto* (Figure 3d, R2,). Nanoparticles were added into a solution of formed, empty frame lattices at 2.5 times excess over the octahedra. Annealing allows for the diffusion/distribution of particles into the ordered scaffold. The resulting S(q) (Figure 3e, blue curve) is in close agreement with route 1. Thus, both routes successfully create the same 3D nanoparticle array. To explore the effect of inter-vertex linkage designs, we varied the ssDNA length and thus the inter-octahedra distance d (Table S1, Figures S14-S15). Well-ordered SC lattices were observed for all but the smallest d values, possibly due to destabilizing electrostatic and steric effects at close separations.

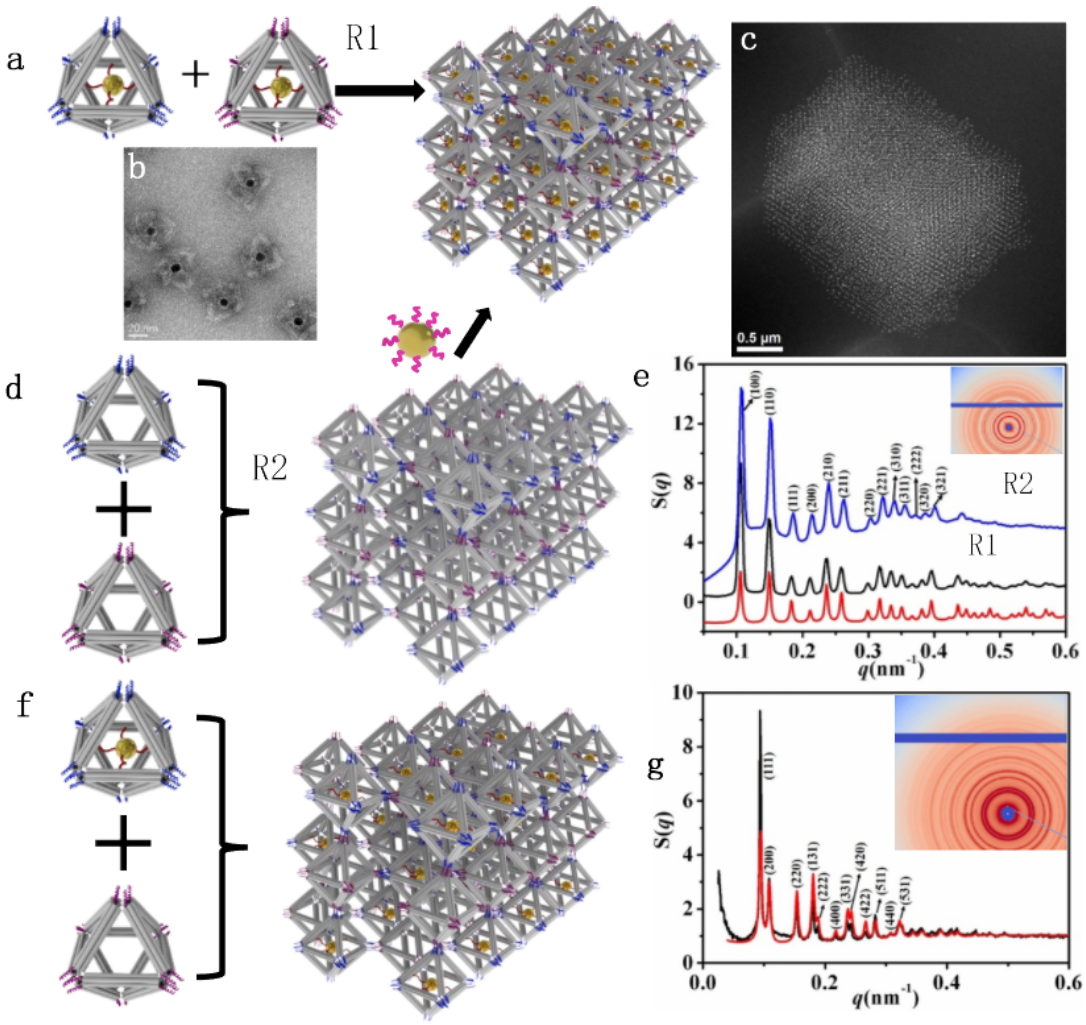

Figure 3. Simple cubic (SC) lattice of gold nanoparticles (AuNP) assembled using material

voxels based on DNA octahedra. (a). Assembly of caged nanoparticles (material voxels) into SC lattice by route 1, R1, first encaging AuNP in DNA frames, followed by frame assembly. Particles are held inside a frame by 8 strands (4 strands are shown for simplicity) (b). Representative TEM image for 10 nm AuNPs encaged by octahedra. (Scale bar: 20 nm) (c). Z-contract annular-dark field Cryo-STEM imaging (Scale bar: 500 nm) for nanoparticle caged 3D superlattice (R1); the same image, analyzed and color-coded for identification of subdomains is shown in Fig. S12, see (Supplementary Material) (d). Assembly by route 2, R2, where empty octahedra first form a lattice, followed by addition of AuNPs to fill the empty lattice through hybridization with strands inside frames. (e). SAXS pattern (inset) and the corresponding structure factor S(q) for lattices of caged AuNP (black curve for R1, blue curve for R2 and red curve for the model, SC with 58.5 nm lattice constant). (f). Assembly of a binary system of octahedral frames with one frame empty and another one hosting AuNP. (g). SAXS pattern (inset) and the related S(q) for the binary lattice shown in (f), where black and red curves correspond to the experimental data and modelling respectively.

To further emphasize this approach's versatility, we can select one of the two types of cages to prefill with nanoparticles while leaving the other empty. Thus, even in the limit of identical DNA cage scaffolds, a totally different nanoparticle superlattice results (Figure 3f). ~20 recognizable SAXS peaks (Figure 3g, black curve), where the peak position ratios q/q_1=1: $\sqrt{4/3}$: $\sqrt{8/3}$:$\sqrt{11/3}$: 2… correspond to a face-centered-cubic (FCC) lattice with lattice constant of 81.2 nm. Detailed S(q) modelling confirms (Figure 3g, red curve) that the nanoparticles are located precisely in every second octahedron in the frame lattice (Fig. 2).

A major advantage of this assembly method is that nano-objects of different kinds can be organized in 3D-ordered arrays in a similar manner. For example, we assembled encaged quantum dots (QD, CdSe, 5 nm core, Figure 4a, inset) using material voxels based on the same type of DNA octahedra. Modelling (see Supplementary Material) shows excellent agreement between the calculated and measured SC S(q) (Figure 4a, red vs. black line; structure illustrated in Figure 4b).

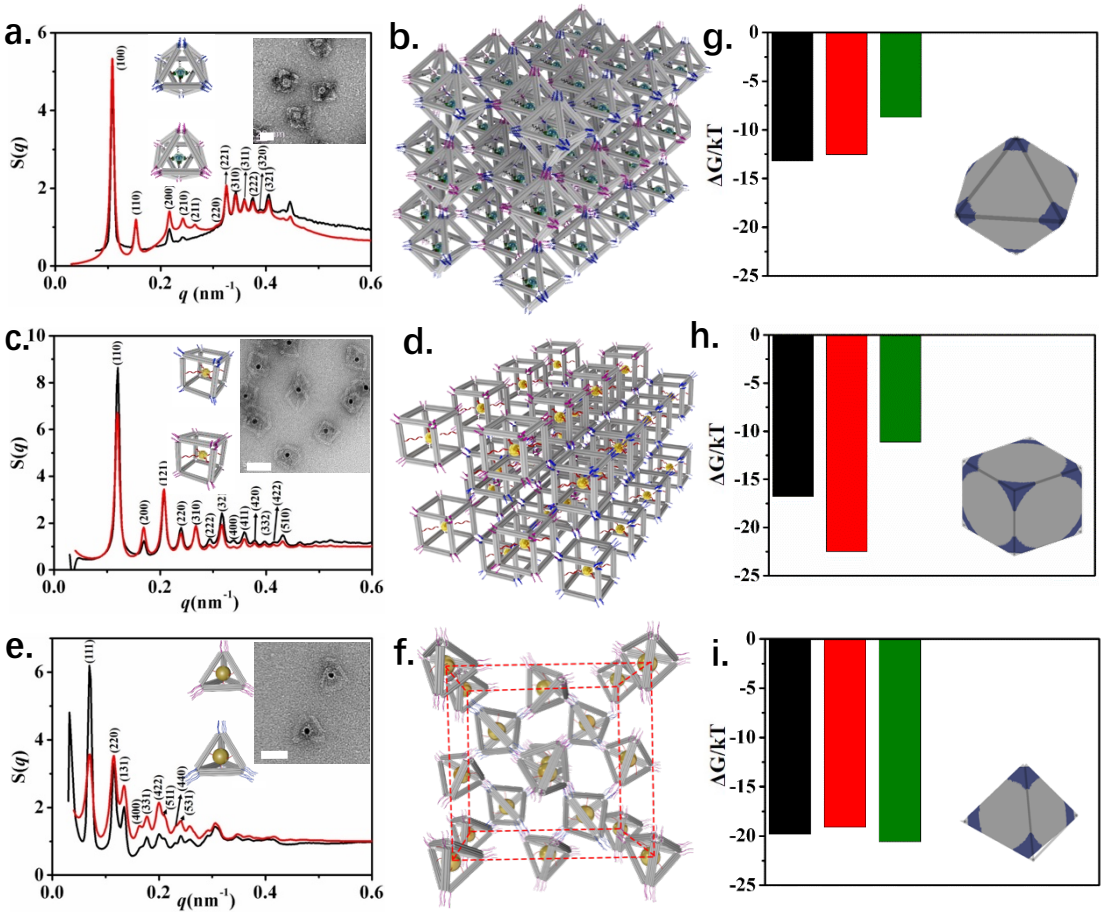

Figure 4. Assembly of nanoparticles from different materials and frames of different geometries into SC, BCC and cubic diamond superlattices. (a). Experimental (black curve) and calculated (red curve) structure factors, S(q), for QDs caged superlattice. Illustration and representative TEM images of individual octahedra (scale bar: 20 nm) with encaged QDs were inserted. (b). An illustration of SC superlattice formed by QDs encaged into octahedra. (c). Experimental (black curve) and calculated (red curve) S(q) for the superlattice of cube encaged AuNP. Illustration and representative TEM images of individual cube (scale bar: 50 nm) with encaged AuNP. (d). Schematics of BCC lattice of vertex-driven assembly of cubes with encaged AuNPs. (e). Experimental (black curve) and calculated (red curve) S(q) for the superlattice of tetrahedron encaged AuNP. Illustration and representative TEM images of individual cube (scale bar: 50 nm) with encaged AuNP. (f). Schematics of cubic diamond lattice of vertex-driven assembly of tetrahedra with encaged AuNPs. (g, h, i). Lattice free energy theoretical prediction per frame for octahedral (g), cubic (h) and tetrahedral (i) systems. Black, red, and green colors relate to SC, BCC, and diamond, respectively. The patchy models of octahedral, cubic, and tetrahedral frames are illustrated, where grey area indicates non-interacting regions and blue patch represents association sites.

This versatile lattice formation strategy can be expanded to create other symmetries using DNA material voxels with different valence. Cubic frames (v=8) composed of

twelve 6HB with edge lengths similar (~29 nm) to the octahedral frames were assembled (Figure S23)[26]. We used two kinds of cubes (CB and CR), where each CB vertex contained three DNA strands complementary to the three CR vertex strands (blue and red in Figure 4c). Both cube populations have another set of DNA sticky-ends at each vertex that point towards the cube center for binding with ssDNA of 10 nm AuNPs. TEM images (Figure 4a and S24) show that the AuNP are encaged with high fidelity; this encapsulation presumably helps to restore cube shape from their skewed empty forms to a normal, undistorted form. Cube assembly was carried out by mixing CB and CR with encaged NPs, followed by annealing as described above. The experimental and model S(q) (Figure 4a, black vs. red curve), reveal a well-ordered body-centered-cubic (BCC) lattice, which is in-line with a vertex-to-vertex hybridization of cubic frames. Considering the nearest interparticle distance (66.2 nm), each CB is connected to CRs at eight vertices yielding the BCC arrangement.

Next we explored assembly of material voxels with v=4 using hybridization between vertices of tetrahedral DNA frames, for which each edge is composed of a 10HB with length ~36 nm[27] (Figure S30) and four internal DNA strands bind 10 nm AuNPs (Figure 4c). Equal amounts of two kinds of tetrahedra possessing complementary sets of 6 sticky-end sequences at their vertices (red (TR) and blue (TB) in Figure 4e) were mixed and annealed. SAXS (Figure 4e) revealed a well-ordered diamond type lattice with ~15 observable scattering peaks (black and red curves). We propose that each tetrahedron binds with four tetrahedra through its vertices (Figure 4f). We stress that this organization is different from our previous report[27], where only particles were arranged in a such lattice and that regime could exist only for the specific size ratio of a frame footprint to a particle. In the current study we observed formation of diamond lattice in respect to frames, thus, inevitably any objects encaged in the frames will form a diamond lattice.

We now theoretically understand the correlation between the DNA frame valence and the resulting lattice. Conventional theories for DNA-mediated self-assembly operate in the limit of high grafting densities and isotropic interaction site distribution[16,28-31]. In

our systems, however, interaction sites are localized to small regions, resulting in "patchy" interframe attractions. We therefore extended Wertheim's thermodynamic perturbation theory for associating particles[32] to properly account for this patchiness. The resulting free energies (see Supplementary information) yield the most favorable ground state crystal structure for a particular frame. We predict that cubic frames preferentially self-assemble into a BCC structure whereas the octahedral frames pack into a SC lattice; diamond lattices are favored for tetrahedral frames. The preference for these morphologies can be explained by decomposing the ΔG into its enthalpic and entropic components, $\Delta G = \Delta H - T\Delta S$ (see Supplementary Material); we find enthalpy dominates. Further, we note that the size and interaction range of these patches strongly depend on the degree of frame truncation; the degree of truncation can be also used to modulate the self-assembled morphologies[33]. These results suggest that truncation tuning could provide an additional powerful handle for expanding this approach to wider ranges of crystal symmetries.

While this theoretical understanding underscores the opportunities in crystal lattice design, we further expand our DNA material voxel assembly strategy by moving beyond inorganic AuNPs and QDs as templated nano-objects to organic materials by creating ordered 3D protein arrays. As an illustration, we use streptavidin, a protein containing four high-affinity sites for biotin binding. We designed 6 hosting sites for streptavidin, one at every vertex of an octahedral DNA frame (v=6), with each site containing 4 ssDNA attached to the 4 corresponding edges that form the vertex (Figure 5a, Supplementary Material). Thus, each streptavidin can bind to biotinylated DNA that is complementary to the edge-attached strands (see Supplementary Material for another example).

The protein-filled material voxels were characterized with cryo-TEM using single particle analysis. 2D class averages of raw particle images are nearly identical to the corresponding reconstructed 3D density model, demonstrating the correct assembly of 6 proteins in the octahedral cage (Figure 5b and Supplementary Material). The cryo-EM 3D map (resolution ~23 Å), allowing for the visualization of the precise protein

positions (Figure 5c), show that the octahedral edge is ~30 nm long, in agreement with our design. The streptavidin lattice structure shows that they are well-docked into six globular densities located at the inner space of vertices. These measurements also indicate full protein occupancy inside cages and high stability of cage-streptavidin complexes.

Subsequently, we mixed OB and OR frames with streptavidin and biotinylated DNA (labeled with Cyanine 3), followed by annealing. We examined the assembled pink-colored aggregates using Confocal Fluorescence Microscopy (CFM) and found fluorescent ~3-5 μm sized square-shapes (Figures 4d and S43). Control experiments mixing OB, OR, and labeled streptavidin, but without biotinylated DNA, showed no fluorescent aggregates, confirming that protein incorporation into DNA frameworks requires specific binding.

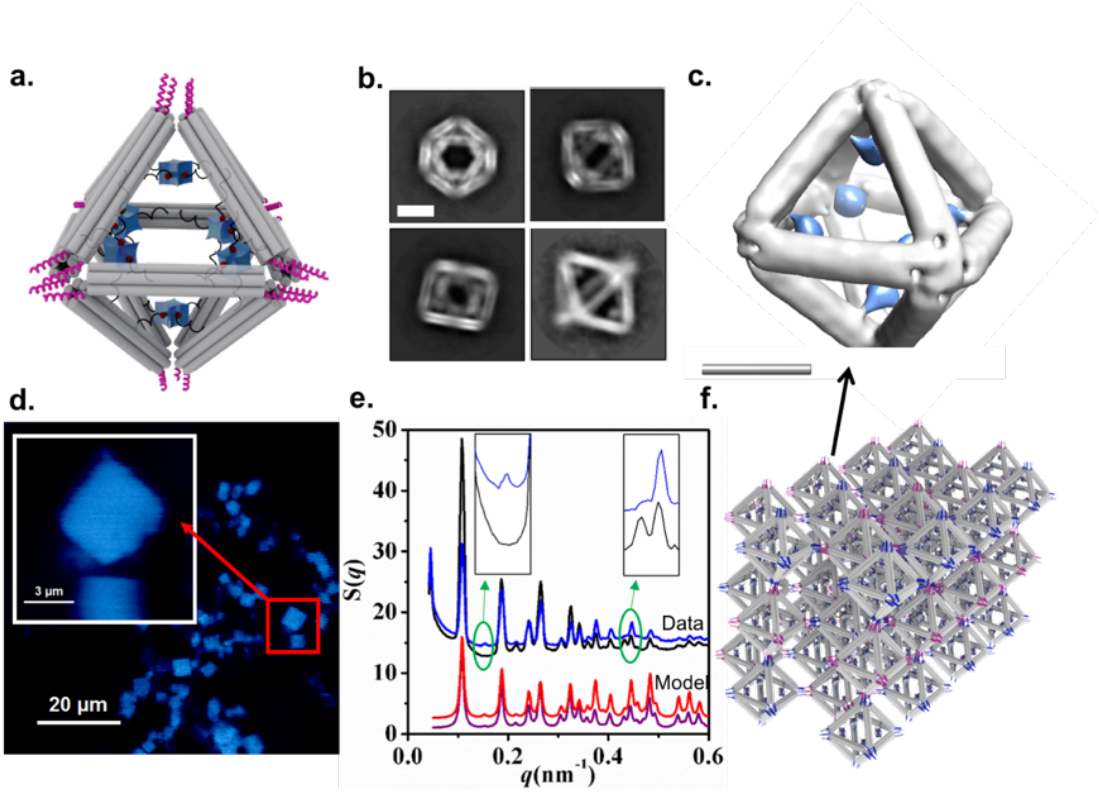

Figure 5. Structure and enzymatic activity of assembled 3D designed lattices (SC) of material voxels with proteins (a). An illustration of encaging of 6 streptavidins inside DNA octahedra. Streptavidins (blue) are placed at the specific prescribed locations, at the inner side of octahedron vertices. (b). Reference-based 2D class average as obtained from cryo-TEM single

particle analysis (scale bar: 20 nm). (c). Cryo-TEM derived 3D density maps of the octahedron encaged proteins. Scale bar: 20 nm. (d). A confocal fluorescent microscopy image of formed crystallites with dye-labeled encaged proteins. (e) Experimental structure factors S(q) for empty DNA 3D lattice (blue curve) and for DNA lattice with 6 proteins placed in a DNA octahedra cage (black curve), as shown in 4a. Respective modelled S(q) for empty (red curve) and protein-filled DNA lattice (purple curve). Green ellipses show zoomed regions where S(q) differs significantly between empty and protein-filled lattice. See Figure S44 for enlarged plots (f). An illustration of assembly of octahedra with encaged 6 streptavidins into 3D superlattice.

SAXS of the encaged streptavidin lattice (Figure 5e) has the same symmetry and peak positions as the corresponding empty DNA cage lattice; moreover, the similar electron density of DNA bundles and streptavidin leads to roughly similar peak intensities for both structures. However, small differences were observed in two highlighted regions of S(q) (Figure 5e). Detailed modelling, accounting for the geometry, locations and density of DNA cages and the 6 encaged streptavidins (Figures 4c and 4f) matches the overall shape of the experimental S(q) for both empty and protein-filled ordered DNA frameworks, and moreover explains the observed differences in S(q). Clearly, protein arrays are templated by an ordered 3D array of octahedral DNA cages.

The confirmation and characterization of different 3D lattices, organizing both inorganic and organic materials, demonstrates the versatility and universality of this DNA material voxel assembly approach. We used this platform to synthesize two different material organizations with properties relevant to dramatically different applications – optical, using a combination of quantum dots, and catalytic, using a cascaded enzyme network organized within a 3D lattice.

Recently, the exploitation of colloidal quantum dot (QD) properties[34] has led to a rapidly growing market for QD-based devices, and even more specifically, QD optoelectronics[35]. The tunability of a CdSe core-shell QD emission has made them an ideal candidate for quantum dot light emitting diodes (QD-LED's)[36,37], which have characteristic high color purity over a color gamut that is far larger than has traditionally been incorporated into display technologies[38]. Such devices are generally formed from layers or films of QD's, yet it has been shown that the photoluminescence quantum yield, η_{PL}, is reduced by 1-2 orders of magnitude in such formats in a field where higher

display brightness is a desired device characteristic [39,40]. The 3D organization of QD's with a controlled, larger separation distance can improve the η_{PL} by reducing energy transfer between QDs. Furthermore, precise control over the structural (unit cell, lattice parameters, etc.) and material properties of 3D QD organizations would allow for the engineering of desired QD superlattice photo-optical responses [41,42].

We programmed 8 distinct binding sites within the interior region of octahedron DNA origami through the use of orthogonal, interior ssDNA overhangs. The OB and OR octahedra were each encoded to host a specific CdSe quantum dot (QD), possessing fluorescence emissions of either 525 or 705 nm, thus resulting in two optically distinctive types of DNA material voxels. ssDNA-modified quantum dots were then annealed into empty, fully-assembled material voxels (v=6) lattices designed to either be half-filled by a single QD or fully-filled by two types of QD's at a 1:1 ratio (materials and methods presented in Supplementary Material and characterization in Figures S52-S60). Fluorescence microscopy imaging and spectra measurements were performed on the QD superlattices, demonstrating a "perfect mixing" of the two fluorescence emissions in superlattices encoded to bind both QDs in equal ratios, Figure 6a. This "perfect mixing" refers to the inability to identify an emission signal from a non-equal QD mixture over a wide range of scan areas down to minimal diffraction-limited scales, Figures 6b and S60, and thus presents a 3D optical organization with sub-diffraction spectral stability. Furthermore, the fluorescence lifetime (τ) of the mixed QD superlattices (Figure S57) was within 15% of superlattices of only one QD for both τ_{525} and τ_{705} (Figures S53 and S55), indicating a minimal energy transfer - a vast improvement over directly layered, thin film systems.

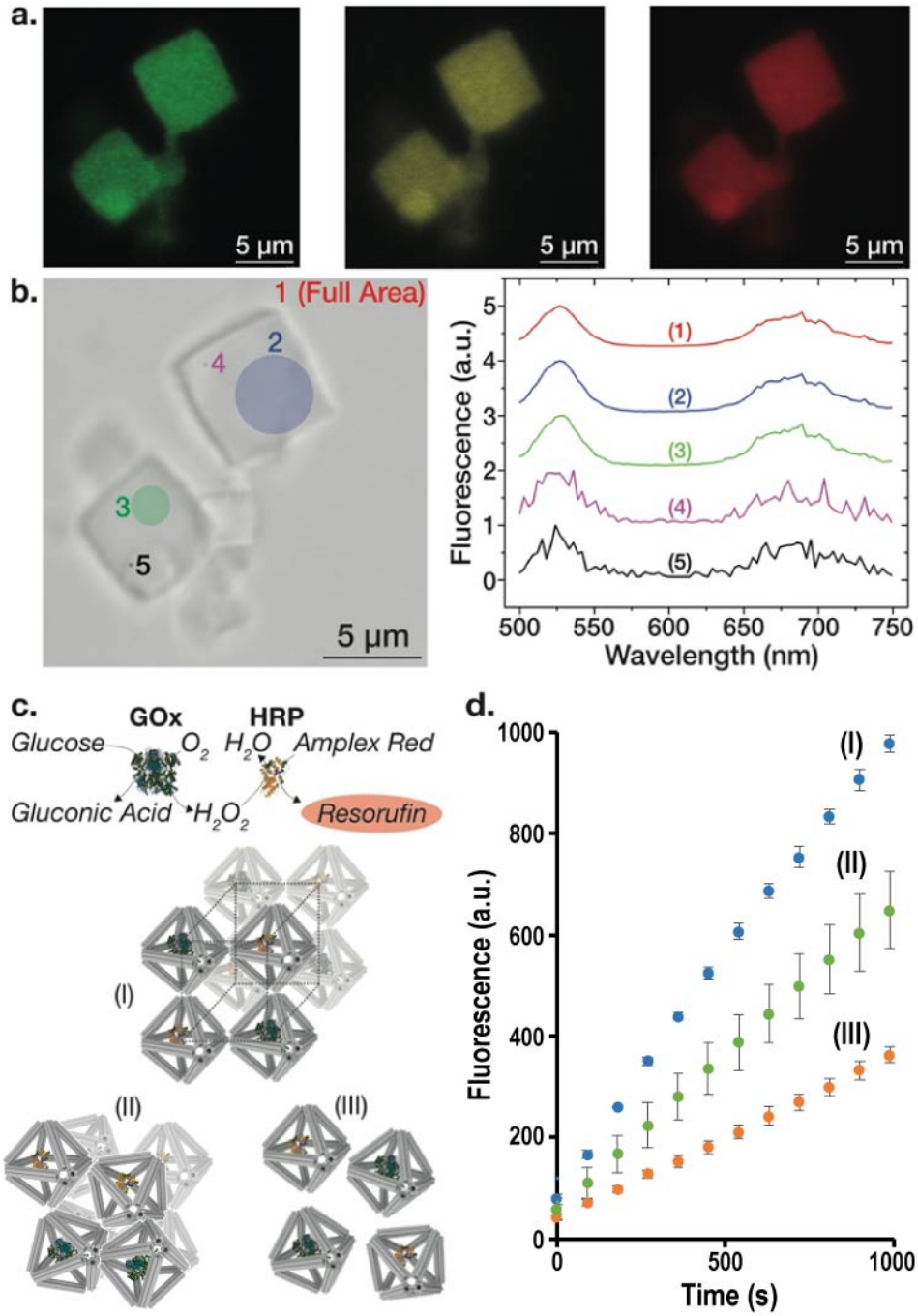

Figure 6. Optical and enzymatic functions of a 3D lattices assembled respectively from DNA material voxels with quantum dots and enzymes. (a). Fluorescence images demonstrating the assembled SC lattice from material voxels (v=6) with QD525 and QD705 (b). Fluorescence profiles over a range of sample analysis areas, demonstrating matching spectral characteristics from an all-sample area down to the diffraction limit. (c). Three different conditions (shown as I, II, III) examined to determine effect of lattice packing and aggregation on the output of an enzymatic cascade consisting of glucose oxidase (GOx) and horseradish peroxidase (HRP) placed inside octahedra. (d). Production of the fluorescent product resorufin from the GOx-HRP reaction is enhanced when in a three-dimensional lattice format.

Next, we demonstrate the catalytic functionality of 3D biomolecular arrays. While previous works have explored the effects of enzyme colocalization in simple geometries and 1D or 2D scaffolds,[43-45] this 3D format provides both significantly denser enzyme packing and a different spatial architecture. We bind ssDNA-modified glucose oxidase (GOx) and horseradish peroxide (HRP), respectively, to a single interior hosting site within each OB and OR octahedra, forming two enzymatic types of material voxels (v=6), which are co-assembled in a lattice as discussed above. The GOx-HRP pair has consistently been used as a model enzymatic cascade[43-45], and here we track it by the synthesis of fluorescent resorufin from the precursor Amplex Red upon glucose addition (reaction overview and sample layout shown in Figure 6c). Equal amounts of origami and enzyme were utilized in each experimental setup to ensure accurate comparisons of activity (see Supplementary Material).

The 3D architecture (I) yields a nearly 300% increase in initial reaction velocities over solution format containing the same concentration of enzyme encaged in free octahedra (III), as shown in Figure 6d. The reaction is undertaken at a concentration of glucose above that needed to achieve V_{max}, as demonstrated by Figure S61a. In order to determine the role of DNA lattice organization itself versus a high local density of origami and enzymes, an associated origami aggregate was formed. This synthesis involved dissociating a lattice prior to enzyme incorporation by heating to 52°C, holding for an hour, and then immediately placing the tube on ice to induce formation of an amorphous assembly. This formation procedure stands in contrast to the controlled, 5 day anneal described in Supplementary Material for an ordered lattice. Sample II in Figure 6d demonstrates that aggregate assembly does induce higher activity than free origami, but not to the extent of an ordered lattice; furthermore, the significantly larger sample variability for amorphous aggregates reflects an intrinsic variability of the disordered states. These results indicate that the lattice architecture does provide a contribution to increased activity of the enzymatic cascade, and not solely aggregation into higher local concentrations. Multiple contributions may play a role in this higher

activity, including high packing density, co-localization of catalytic components, and local environment effects of the DNA framework. While the specific contributions of each of these effects call for detailed mechanistic studies, this work shows an ability to structure enzymes into active high-density 3D arrays using material voxel strategy, and possibility for manipulating and enhancing cascade reactions using such 3D packaging of enzymes.

In summary, we demonstrated the assembly platform for creating 3D lattices from nanomaterials of different natures, both inorganic and bio-organic, as well as stand-alone DNA origami frames. Our approach integrates DNA frames with a prescribed valence and material nano-objects into a material voxel. That allows us defining a lattice symmetry and a lattice composition through the material voxel design and enable nanomaterials with novel optical and chemical properties. The presented strategy offers a powerful pathway for the rational assembly of 3D ordered nanomaterials from desired nano-objects for a broad range of applications.

Acknowledgments

We thank W. Xia for help with cryo-STEM imaging, M. Ji for help with negative stained TEM imaging, Y. Zhang and A. Fluerasu for help with SAXS measurement at the CHX beamline (NSLS-II at the Brookhaven National Laboratory), M. Cotlet and J. Chen for help with optical characterization, and D. Chen for help with illustrations. Cryo-TEM data was collected at the David Van Andel Advanced Cryo-Electron Microscopy Suite in the Van Andel Research Institute. HL was supported by the US National Institutes of Health (GM111472 and GM124170) and the Van Andel Research Institute. This research used resources of the Center for Functional Nanomaterials, and the National Synchrotron Light Source II, which are U.S. DOE Office of Science Facilities at Brookhaven National Laboratory under Contract No. DE-SC0012704. This work was supported by the US Department of Energy, Office of Basic Energy Sciences, grant DE-SC0008772.

References

1 Jones, M. R., Macfarlane, R. J., Lee, B., Zhang, J. A., Young, K. L., Senesi, A. J. & Mirkin, C. A. DNA-nanoparticle superlattices formed from anisotropic building blocks. *Nature Materials* **9**, 913-917, doi:10.1038/NMAT2870 (2010).

2 Lu, F., Yager, K. G., Zhang, Y. G., Xin, H. L. & Gang, O. Superlattices assembled through shape-induced directional binding. *Nature Communications* **6**, doi:Artn 6912
10.1038/Ncomms7912 (2015).

3 Agarwal, U. & Escobedo, F. A. Mesophase behaviour of polyhedral particles. *Nat Mater* **10**, 230-235, doi:10.1038/NMAT2959 (2011).

4 Gantapara, A. P., de Graaf, J., van Roij, R. & Dijkstra, M. Phase Diagram and Structural Diversity of a Family of Truncated Cubes: Degenerate Close-Packed Structures and Vacancy-Rich States. *Phys Rev Lett* **111**, doi:Artn 015501
10.1103/Physrevlett.111.015501 (2013).

5 Talapin, D. V., Shevchenko, E. V., Bodnarchuk, M. I., Ye, X. C., Chen, J. & Murray, C. B. Quasicrystalline order in self-assembled binary nanoparticle superlattices. *Nature* **461**, 964-967, doi:10.1038/nature08439 (2009).

6 Damasceno, P. F., Engel, M. & Glotzer, S. C. Predictive Self-Assembly of Polyhedra into Complex Structures. *Science* **337**, 453-457, doi:10.1126/science.1220869 (2012).

7 Seeman, N. C. Nucleic Acid Junctions and Lattices. *J. theor. Biol.*, 237-247 (1982).

8 Chen, J. & Seeman, N. C. Synthesis from DNA of a molecule with the connectivity of a cube. *Nature* **350**, 631-633 (1991).

9 Rothemund, P. W. K. Folding DNA to create nanoscale shapes and patterns. *Nature* **440**, 297-302 (2006).

10 He, Y., Ye, T., Su, M., Zhang, C., Ribbe, A. E., Jiang, W. & Mao, C. Hierarchical self-assembly of DNA into symmetric supramolecular polyhedra. *Nature* **452**, 198-201 (2008).

11 Seeman, N. C. DNA in a material world. *Nature* **421**, 427-431 (2003).

12 Halverson, J. D. & Tkachenko, A. V. DNA-programmed mesoscopic architecture. *Phys. Rev. E* **87**, 062310 (2013).

13 Zheng;, J., Constantinou;, P. E., Micheel;, C., Alivisatos;, A. P., Kiehl;, R. A. & Seeman;, N. C. Two-Dimensional Nanoparticle Arrays Show the Organizational Power of Robust DNA Motifs. *Nano Letters* **6**, 1502-1504 (2006).

14 Nykypanchuk, D., Maye, M. M., van der Lelie, D. & Gang, O. DNA-guided crystallization of colloidal nanoparticles. *Nature* **451**, 549-552 (2008).

15 Park, S. Y., Lytton-Jean, A. K. R., Lee, B., Weigand, S., Schatz, G. C. & Mirkin, C. A. DNA-programmable nanoparticle crystallization. *Nature* **451**, 553-556 (2008).

16 Vo, T., Venkatasubramanian, V., Kumar, S., Srinivasan, B., Pal, S., Zhang, Y. G. & Gang, O. Stoichiometric control of DNA-grafted colloid self-assembly. *Proc. Natl. Acad. Sci. USA* **112**, 4982-4987 (2015).

17 Niemeyer, C. M., Koehler, J. & Wuerdemann, C. DNA-directed assembly of bienzymic complexes from in vivo biotinylated NAD(P)H:FMN oxidoreductase and luciferase. *ChemBioChem*, 242-245 (2002).
18 Lee, J. B., Peng, S., Yang, D., Roh, Y. H., Funabashi, H., Park, N., Rice, E. J., Chen, L., Long, R., Wu, M. & Luo, D. A mechanical metamaterial made from a DNA hydrogel. *Nat. Nanotechnol.* **7**, 816-820 (2012).
19 Church, G. M., Gao, Y. & Kosuri, S. Next-Generation Digital Information Storage in DNA. *Science* **337**, 1628 (2012).
20 Zheng, J., Birktoft, J. J., Chen, Y., Wang, T., Sha, R., Constantinou, P. E., Ginell, S. L., Mao, C. & Seeman, N. C. From molecular to macroscopic via the rational design of a self-assembled 3D DNA crystal. *Nature* **461**, 74-77 (2009).
21 Wang, X., Sha, R., Kristiansen, M., Hernandez, C., Hao, Y., Mao, C., Canary, J. W. & Seeman, N. C. An organic semiconductor organized into 3D DNA arrays by 'bottom-up' rational design. *Angew. Chem. Int. Edit.* **56**, 6445-6448 (2017).
22 Hao, Y., Kristiansen, M., Sha, R., Birktoft, J. J., Hernandez, C., Mao, C. & Seeman, N. C. A device that operates within within a self-assembled 3D DNA crystal. *Nat. Chem.* (2017).
23 Douglas, S. M., Dietz, H., Liedl, T., Hogberg, B., Graf, F. & Shih, W. M. Self-assembly of DNA into nanoscale three-dimensional shapes. *Nature* **459**, 414-418 (2009).
24 Zhang, T., Hartl, C., Frank, K., Heuer-Jungemann, A., Fischer, S., Nickels, P. C., Nickel, B. & Liedl, T. 3D DNA Origami Crystals. *Advanced Materials* **30**, 1800273, doi:10.1002/adma.201800273 (2018).
25 Yager, K. G., Zhang, Y. G., Lu, F. & Gang, O. Periodic lattices of arbitrary nano-objects: modeling and applications for self-assembled systems. *Journal of Applied Crystallography* **47**, 118-129, doi:Doi 10.1107/S160057671302832x (2014).
26 Tian, Y., Zhang, Y., Wang, T., Xin, H. L., Li, H. & Gang, O. Lattice engineering through nanoparticle–DNA frameworks. *Nat. Mater.* **15**, 654-661 (2016).
27 Liu, W., Tagawa, M., Xin, H. L., Wang, T., Emamy, H., Li, H., Yager, K. G., Starr, F. W., Tkachenko, A. V. & Gang1, O. Diamond family of nanoparticle superlattices. *Science* **351**, 582-586, doi:10.1126/science.aad2080 (2016).
28 Macfarlane, R. J., Lee, B., Jones, M. R., Harris, N., Schatz, G. C. & Mirkin, C. A. Nanoparticle superlattice engineering with DNA. *Science* **334**, 204-208 (2011).
29 Rogers;, W. B. & Crocker;, J. C. Direct measurements of DNA-mediated colloidal interactions and their quantitative modeling. *Proceedings of the National Academy of Sciences* **108**, 15687–15692 (2011).
30 Varilly;, P., Angioletti-Uberti;, S., Mognetti;, B. M. & Frenkel;, D. A general theory of DNA-mediated and other valence-limited colloidal interactions. *The Journal of Chemical Physics* **137**, 094108 (2012).
31 Travesset, A. Binary nanoparticle superlattices of softparticle systems. *Proc. Natl. Acad. Sci. USA* **112**, 9563–9567 (2015).
32 MS, W. Fluids with highly directional attractive forces. iii. multiple attraction

sites. *J. Stat. Phys* **42**, 459–476 (1986).
33 Damasecno, P. F., Engel, M. & Glotzer, S. C. Crystalline assemblies and densest packings of a family of truncated tetrahedra and the role of directional entropic forces. *ACS Nano* **6**, 609-614 (2012).
34 Murray, C. B., Kagan, C. R. & Bawendi, M. G. Synthesis and Characterization of Monodisperse Nanocrystals and Close-Packed Nanocrystal Assemblies. *Annual Review of Materials Science* **30**, 545-610, doi:10.1146/annurev.matsci.30.1.545 (2000).
35 Oliver, J. Quantum Dots: Global Market Growth and Future Commercial Prospects
. *BCC Research* **NAN027E** (2016).
36 Jang, E., Jun, S., Jang, H., Lim, J., Kim, B. & Kim, Y. White-Light-Emitting Diodes with Quantum Dot Color Converters for Display Backlights. *Advanced Materials* **22**, 3076-3080, doi:10.1002/adma.201000525 (2010).
37 Kim, T.-H., Cho, K.-S., Lee, E. K., Lee, S. J., Chae, J., Kim, J. W., Kim, D. H., Kwon, J.-Y., Amaratunga, G., Lee, S. Y., Choi, B. L., Kuk, Y., Kim, J. M. & Kim, K. Full-colour quantum dot displays fabricated by transfer printing. *Nature Photonics* **5**, 176, doi:10.1038/nphoton.2011.12
https://www.nature.com/articles/nphoton.2011.12#supplementary-information (2011).
38 Wood, V. & Bulović, V. Colloidal quantum dot light-emitting devices. *Nano Reviews* **1**, 5202, doi:10.3402/nano.v1i0.5202 (2010).
39 Chang, T.-W. F., Maria, A., Cyr, P. W., Sukhovatkin, V., Levina, L. & Sargent, E. H. High near-infrared photoluminescence quantum efficiency from PbS nanocrystals in polymer films. *Synthetic Metals* **148**, 257-261, doi:https://doi.org/10.1016/j.synthmet.2004.10.003 (2005).
40 Kagan, C. R., Murray, C. B., Nirmal, M. & Bawendi, M. G. Electronic Energy Transfer in CdSe Quantum Dot Solids. *Physical Review Letters* **76**, 1517-1520, doi:10.1103/PhysRevLett.76.1517 (1996).
41 Baimuratov, A. S., Rukhlenko, I. D., Turkov, V. K., Baranov, A. V. & Fedorov, A. V. Quantum-dot supercrystals for future nanophotonics. *Scientific Reports* **3**, 1727, doi:10.1038/srep01727 (2013).
42 Kim, D., Tomita, S., Ohshiro, K., Watanabe, T., Sakai, T., Chang, I. Y. & Hyeon-Deuk, K. Evidence of Quantum Resonance in Periodically-Ordered Three-Dimensional Superlattice of CdTe Quantum Dots. *Nano Letters* **15**, 4343-4347, doi:10.1021/acs.nanolett.5b00335 (2015).
43 Wilner, O. I., Weizmann, Y., Gill, R., Lioubashevski, O., Freeman, R. & Willner, I. Enzyme cascades activated on topologically programmed DNA scaffolds. *Nature Nanotechnology* **4**, 249-249 (2009).
44 Fu, J., Liu, M., Liu, Y., Woodbury, N. W. & Yan, H. Interenzyme Substrate Diffusion for an Enzyme Cascade Organized on Spatially Addressable DNA Nanostructures. *Journal of the American Chemical Society* **134**, 5516-5519, doi:10.1021/ja300897h (2012).
45 Zhao, Z., Fu, J., Dhakal, S., Johnson-Buck, A., Liu, M., Zhang, T., Woodbury, N. W., Liu, Y., Walter, N. G. & Yan, H. Nanocaged enzymes with enhanced

catalytic activity and increased stability against protease digestion. *Nature Communications* **7**, 10619-10619 (2016).